UNIVERSITY *of York*

This is a repository copy of *Commonality of Virulence-Promoting Function in Rhodococcus equi Virulence Associated Proteins (Vaps)*.

White Rose Research Online URL for this paper:
https://eprints.whiterose.ac.uk/204174/

Version: Published Version

Article:

White Rose
university consortium
Universities of Leeds, Sheffield & York

eprints@whiterose.ac.uk
https://eprints.whiterose.ac.uk/

WILEY | Hindawi

Research Article

Commonality of Virulence-Promoting Function in *Rhodococcus equi* Virulence Associated Proteins (Vaps)

Timothy R. Ganderton [iD],[1] **Daniel Ghete** [iD],[2] **Karen Hogg** [iD],[2] **Graeme J. Park** [iD],[2] **Christoph G. Baumann** [iD],[3] **Anthony J. Wilkinson** [iD],[4] **and Paul R. Pryor** [iD][1]

[1]Experimental Medicine and Biomedicine Unit, Hull York Medical School & York Biomedical Research Institute, University of York, YO10 5DD, UK
[2]Bioscience Technology Facility, Department of Biology, University of York, YO10 5DD York, UK
[3]Department of Biology, University of York, YO10 5DD York, UK
[4]York Structural Biology Laboratory & York Biomedical Research Institute, Department of Chemistry, University of York, YO10 5DD, UK

Correspondence should be addressed to Paul R. Pryor; paul.pryor@york.ac.uk

Rhodococcus equi is a Gram-positive facultative intracellular pathogen associated with life-threatening bronchopneumonial disease in foals. Key to *R. equi's* intracellular survival in host macrophages is the production of virulence associated proteins (Vaps). Numerous *vap* genes are found on virulence plasmids isolated from different species, and the Vaps share a high degree of sequence identity. VapA has been extensively studied, and although *vapK* and *vapN* genes from other *R. equi* virulence plasmids have been shown to be essential for *R. equi* intracellular survival, their mode of action is less characterised. We, therefore, examined whether VapK and VapN worked mechanistically in the same way as VapA. Indeed, like VapA, VapK and VapN neutralised lysosomal pH and reduced lysosomal hydrolase activity. A loss of VapA and *R. equi* virulence could be regained by the presence of either VapK or VapN. The acid-neutralisation activity was also observed to a lesser extent with VapB. There was a differential activity across these virulence-promoting Vaps with the most "acid-neutralising" activity found with VapN, then VapA and K, and finally VapB. These data suggest that VapA production, which is often found in equine infections, can be substituted by VapK and B (produced by plasmids often found in porcine species) or VapN (produced by plasmids often isolated in bovine and human samples). These data imply that the molecular mechanism(s) that VapA uses to neutralise lysosomal acidity should also be seen in VapN and K which will help guide researchers in identifying their precise mode of action and aid the future development of targeted therapeutics.

1. Introduction

Rhodococcus equi (*R. equi*) is a soil-dwelling pathogenic actinomycete that causes pulmonary and extrapulmonary pyogranulomatous infections in a variety of animal species [1]. *R. equi* infects various animal hosts, including pigs, sheep, cattle, goats [2], and camelids [3] but is most frequently associated with life-threatening bronchopneumonial disease in foals [4]. *R. equi* is prevalent on horse-breeding farms worldwide and has a significant economic impact on the horse-breeding industry [5]. Treatments for *R. equi* infections involve combi-

nation drug therapies with rifampin and macrolides such as clarithromycin [6]. These treatments can be protracted and expensive; moreover, they are not always successful, and there is increasing antibiotic resistance [7–11]. Additionally, *R. equi* is increasingly isolated from immunocompromised humans [12–16], and antibiotic-resistant strains of *R. equi* represent a further threat to human health because of the risk of zoonotic transmission.

Alveolar macrophages phagocytose *R. equi* that then become enclosed in an intracellular compartment termed the *R.equi*-containing vacuole (RCV) in which the bacterium

survives and begins to multiply eventually resulting in necrosis of the host cell [17]. Essential for *R. equi* survival is a virulence plasmid whose prevalence varies according to host species [18–24]. pVAPA, the first of these plasmids to be discovered, is generally associated with equine *R. equi* isolates. pVAPB is mostly closely linked to porcine *R. equi* infections while pVAPN is often found in *R. equi* in bovine and human isolates. Plasmid swapping (pVAPA for pVAPB) does not affect *R. equi* virulence in swine or equine macrophages [25].

The virulence plasmids of *R. equi* contain a pathogenicity island comprising multiple genes encoding virulence-associated proteins (Vaps). pVAPA encodes VapA, VapC, VapD, VapE, VapG, and Vap H. It also harbours three pseudogenes (*vapF, I,* and *X*). pVAPB encodes VapB, VapJ, VapK1, VapK2, VapL, and VapM, while pVAPN encodes VapN, VapO, VapP, and VapQ (a pseudogene), VapR, and VapS [24]. VapA alone among the Vaps encoded by pVAPA is necessary for *R. equi* virulence [19, 26, 27]. Two transcriptional regulators VirR and VirS are also important virulence determinants [28, 29]. For *R. equi* isolates harbouring pVAPN, it is the *vapN* gene from the *vap* genes, which is essential for virulence [23]. Meanwhile, in isolates carrying pVAPB, the genes *vapK1 and vapK2* (VapK1 and VapK2 differ by a single amino acid) are essential for virulence; moreover, these genes can restore virulence in *ΔvapA* strains [30]. This suggests strongly that VapK1/2 is the functional homolog of VapA, despite VapB having a higher degree of homology to VapA.

The Vaps possess N-terminal secretion signals consistent with their export from the bacterial cell giving rise to mature proteins of 130-160 amino acid residues. Sequence alignment of the different Vap proteins shows that they share a high degree of homology in the last 110 or so amino acids with little homology in the preceding 25-40 residues at the N-terminus. The crystal structures of the C-terminal regions, which we refer to here as the core domain, of VapB, VapD, and VapG have been determined by X-ray crystallography [31–33] revealing a tightly packed eight-stranded β-barrel. The structures of these three Vaps are closely superimposable. Alphafold [34] indicates that the structures of the other Vaps will be very similar to the crystal structures of VapB, D, and G. Conspicuously absent from the crystal structures of the Vaps are obvious cavities or grooves that might represent a ligand binding site that would provide clues to their function.

What is apparent is that VapA disrupts endolysosomes [35] so that lysosomes are not reformed, and this disruptive activity can be accounted for by VapA's capacity to reduce the acidity of the endolysosomal compartment [36–38]. Given the high degree of sequence identity across Vaps and the predicted similarities in their structures, we wanted to identify what features VapA possesses that are absent from the Vaps that do not promote *R. equi* virulence. Further, we wished to examine whether VapK and VapN (the reported equivalents of VapA) work in the same way as VapA, given that properties of VapA, such as the binding to phosphatidic acid [39], were not seen with VapK.

Our results indicate that VapA, K, and N work in a similar manner and that late endocytic compartment acidity

is reduced, leading to a loss of lysosomal hydrolytic activity. This activity is also seen to a certain extent with VapB, which has the highest degree of homology to VapA. These data imply that the mechanism(s) that Vaps use to neutralise lysosomal acidity should be seen in VapA, K, and N which will guide researchers in identifying their precise mode of action and aid in the future development of targeted therapeutics.

2. Methods

2.1. Reagents and Antibodies. Mouse anti-rat LGP120 (GM10) was a kind gift from Prof. J. Paul Luzio (University of Cambridge, UK). Primary antibodies: *a*-tubulin (Sigma clone DM1A), LC3 (Nanotools 5F10) ATP6V$_1$D (Abcam ab157458), ATP6V$_0$a3 (Invitrogen PA5-90425), ATP6V$_0$d (Abcam ab202899), ATP6V$_1$A (Abcam ab199326), ATP6V$_1$B (Abcam 200839), ATP6V$_1$D (Abcam ab157458), ATP6V$_1$E1 (Invitrogen PA529899), 1D4B (Developmental Studies Hybridoma Bank (DSHB); rat anti-mouse Lamp1), 6XHis (Thermo-Fisher Scientific MA1-21315). Alexa-Fluor labelled secondary antibodies were from Invitrogen. HRP-labelled secondary antibodies (A9169, A9044, A9542), Bafilomycin-A$_1$ (B1793), Concanamycin-A (C9705), ATP (20-306), NADH (N8129), phosphoenol pyruvate (101082940), and pyruvate kinase/lactate dehydrogenase (P0294) were all purchased from Merck. LysoTracker-Red DND-99 and DQ-Red BSA were both purchased from Thermo Fisher Scientific.

2.2. R. equi. All *R. equi* strains 103+, plasmid-less 103- and 103+ *ΔvapA* were kind gifts from Wim Meijer (University College Dublin).

2.3. Cell Culture. Normal rat kidney (NRK) and NRK lgp120-GFP cells (a gift from Paul Luzio) were cultured in DMEM (Sigma) supplemented with 10% (v/v) FBS (Gibco), 1% (v/v) glutamine and Pen/Strep (Sigma) +500 μg/mL G418 (Gibco) for lgp120-GFP lines. J774A.1 (murine monocyte/macrophage; ECACC) cells were cultured in DMEM supplemented with 10% (v/v) heat-inactivated (65°C for 20 min) FBS and glutamine. All cells were grown at 37°C/5% CO$_2$. Only J774A.1 cells with a passage number of less than 20 were used in experiments.

2.4. Protein Alignments. Protein identity percentages were obtained from multiple sequence alignments using Clustal Omega (https://www.ebi.ac.uk/Tools/msa/clustalo/). Heat maps were generated using GraphPad Prism. Sequences used for alignments are in supplementary data.

2.5. Immunofluorescence. NRK or J774A.1 cells were seeded onto coverslips (no. 1.5, Scientific Laboratory Supplies) and incubated overnight. If cells were fed purified proteins, then NRK cells were fed protein at 40 μg/ml (unless otherwise stated) and J774A.1 at 5 μg/mL (unless otherwise stated) for 20 h. If J774A.1 were infected with *R. equi,* then cells were treated as per the infection assay but fixed instead of lysed at appropriate times. Coverslips were rinsed with PBS, fixed in 4% (w/v) formaldehyde (04018-1, Polysciences Inc.) for 20 min, incubated in 40 mM NH$_4$Cl (Sigma) for

10 min, and then permeabilised with BSP (0.2% (w/v) BSA (Fraction V, Roche), 0.05% (w/v) saponin (S4521, Sigma) in PBS) for 10 min. Coverslips were incubated with primary antibodies in BSP for 1 h, washed 3×5 min with BSP, and then incubated with secondary antibodies in BSP for 30 min. Coverslips were washed 3×5 min with BSP, rinsed in deionised H_2O, and mounted onto slides with MOWIOL 4–88 (Sigma) containing 2.5% (w/v) DABCO (1,4-diazobi-cyclo[2,2,2]-octane; Sigma). Where appropriate, DNA was stained with $4'$,6-diamidino-2-phenylindole (DAPI, Sigma) at $1 \mu g/ml$ in the final wash before mounting. Cells were imaged using a Zeiss 880 Axioscan confocal microscope (unless otherwise stated). All images are maximum intensity z-projections. Images were processed using ImageJ (v 2.1.0/1.53c).

2.6. Protein Expression and Purification.

All genes expressing the Vaps' core region (see supplementary data for sequences) were cloned into pET30b or pET26a expression vectors (Novagen) with all proteins having a C-terminal His$_6$-tag (Novagen). Genes for *vapK* and *vapN* were synthesised by GeneArt (ThermoScientific) using codon optimisation for expression in *E.coli*. VapA-pHluorin2 was made by cloning pHluorin2 from pME pHluorin2 (Addgene #73794) downstream of VapA in pET26a. BL21 (DE3) cells (Agilent Technologies) transformed with expression plasmids were grown in lysogeny broth (LB; Oxoid) with $50 \mu g/ml$ kanamycin (Sigma), and expression was induced with 0.5 mM IPTG (Melford Laboratories) at an OD_{600} between 0.7 and 0.9. Cells were harvested by centrifugation at 4 h postinduction, and cell pellets were resuspended in lysis buffer (30 mM Tris pH 8, 500 mM NaCl, 30 mM imidazole, $200 \mu g/mL$ lysozyme, $100 \mu g/mL$ DNase, 1 mM $MgCl_2$; all components from Sigma) and stored at -20°C before further processing. Cell lysates were clarified by centrifugation (30 min, $4,700 g$), and the supernatant passed over a 2 mL HisTrap column (G.E. Healthcare) equilibrated with wash buffer (30 mM Tris pH 8, 500 mM NaCl, 30 mM imidazole). The column was washed with 20 column volumes of wash buffer, and the protein was eluted with 5 column volumes of wash buffer containing 500 mM imidazole. Eluates were concentrated using a Centricon with a 3,000 MWCO (Merck Millipore) before size exclusion chromatography using a S75 increase column (G.E. Healthcare) in 30 mM Tris, pH 8, and 500 mM NaCl. All proteins used retained the His$_6$-tag. Protein purity was assessed by SDS-PAGE, and purified proteins snap frozen and stored at -80°C.

2.7. Infection Assay.

With the exception of blood heart infusion (BHI; Sigma), all media, buffers, and reagents were kept at 37°C. J774A.1 cells were infected with *R. equi* strains at an MOI of 10. On day 1, J774A.1 cells were seeded into 24-well plates at 5×10^5 cells/well and incubated overnight at 37°C/5%CO$_2$, and *R. equi* strains were grown overnight in liquid BHI at 30°C. On day 2, fresh BHI was inoculated with the overnight cultures of *R. equi* to an OD_{600} of 0.1, and cultures grown until they reached an OD_{600} of 0.6 (approx. 3 h), after which they were diluted to an OD_{600} of 0.1 in warm DMEM (10% (v/v) heat-inactivated FBS) without and with recombinant Vaps (1 or $5 \mu g/ml$). Media on J774A.1 cells were replaced with *R. equi* (-/+ Vaps). The plates were centrifuged at 300 g for 3 min and incubated for 1 h at 37°C/5%CO$_2$. After 1 h macrophage cells were gently washed twice with warm PBS, then fresh warm DMEM was added to the cells (-/+ Vap protein), and they were incubated for 2 h at 37°C/5%CO$_2$. After 2 h, the DMEM was aspirated and replaced with fresh DMEM (-/+ Vap protein) containing $3 \mu g/ml$ vancomycin (Sigma) and plates incubated at 37°C/5% CO$_2$. At 8 and 24 h postinfection, plates were removed from the incubator, media aspirated, cells washed gently with warm PBS, and then lysed with sterile 0.1% (v/v) Triton X-100 (Sigma) in deionised H_2O. Lysates were vortexed, diluted 1000-fold with deionised H_2O, and spread onto warm BHI agar (Sigma) plates. Colonies (cfu) were counted after 48 h incubation at 37°C to determine cfu/well. For each experiment, a separate 24-well plate was used for each time point, three wells per plate were used for each treatment, and the lysate from each well was plated separately. Data used in statistical analyses were collected from at least 3 independent experiments per treatment.

2.8. Flow Cytometry.

5×10^5 J774.2 cells/well were seeded into 24 well plates and allowed to semi-adhere for 24 h. Cells were incubated with Vaps ($5 \mu g/ml$) or bafilomycin-A$_1$ (100 nM; Sigma) for 24 h before the addition of 50 nM Lyso-Tracker Red DND-99 for 30 min at 37°C. Cells were gently rinsed with PBS at 37°C and resuspended by pipetting into PBS containing DAPI ($1 \mu g/ml$) before flow cytometry analyses. LysoTracker accumulation in cells was measured by a Beckman Coulter CytoFLEX S flow cytometer using a 561 nm laser and the detection channel 585/42. Cells were gated by live cells (DAPI exclusion) using a 405 nm laser and the detection channel 450/45, and single cells using 488 nm laser height and area side scatter signals. Data from 5×10^3 cells were recorded for all samples. For DQ-BSA experiments, cells were treated as above, but instead of Lyso-Tracker, cells were incubated with $10 \mu g/ml$ DQ Red-BSA for 1.5 h; then, medium was changed for DQ-BSA-free medium at 37°C for 1 h before analysis on the CytoFLEX S (as for LysoTracker).

2.9. Isolation of Lysosomes.

Macrophages were incubated $\pm 5 \mu g/ml$ VapA for 20 h before isolation of lysosomes as previously described [40]. Briefly, macrophages are pulsed for 1 h with colloidal iron-dextran before being chased for 2 h by media without dextran. Cells are then gently broken by nitrogen cavitation, and a postnuclear supernatant (PNS) is generated. The PNS is then passed through an iron-filings column in the presence of a strong magnetic field, retaining the iron-filled lysosomes, and then the lysosomes are eluted from the column by removal of the magnetic field.

2.10. V-ATPase Assay.

Isolated lysosomes (from the equivalent of $4 \times 175 cm^2$ tissue culture flasks) were pelleted at 100,000 g for 15 min and then resuspended in 1 ml of assay buffer (50 mM K$^+$-HEPES, pH 7.5, 120 mM K$^+$-acetate, 8 mM Mg^{2+}-acetate, $20 \mu l/ml$ phosphoenolpyruvate/NAD mix (9.4 mg phosphoenolpyruvate, 2 mg NADH in $200 \mu l$ 50 mM Tris, pH 8.0 made fresh), $10 \mu l$ pyruvate kinase/

lactate dehydrogenase mix (see reagents), 5 mM sodium azide (Sigma), and $\pm 1\,\mu l$ concanamycin-A. $200\,\mu l$ aliquots were placed into a 96-well plate and incubated for 30 min at 37°C. Reactions were started by rapidly adding $4\,\mu l$ of 100 mM ATP to each well. Using a BMG CLARIOstar plate reader with shaking, NADH fluorescence (which reduces upon oxidation) was measured every minute (Ex = 340/15 nm, Dichroic = 398.8 nm, Em = 460/20 nm).

2.11. Holotomography. For holotomography, 1 h before the start of imaging, cells were put into a heated CO_2 chamber on the microscope to equilibrate. Three-dimensional (3D) quantitative phase imaging (QPI) and its correlative fluorescence images of live LGP120-GFP NRK cells were obtained using a commercial holotomography instrument (HT-2H, Tomocube), which is based on the Mach–Zehnder interferometry equipped with a digital micromirror device. A coherent monochromatic laser ($\lambda = 532$ nm) was divided into two paths, a reference and a sample beam, respectively, using a 2×2 single-mode fibre coupler. A 3D RI tomogram was reconstructed from multiple 2D holographic images acquired from 49 illumination conditions, a normal incidence, and 48 azimuthally symmetric directions with a polar angle (64.5°). The digital micromirror device was used to control the angle of an illumination beam impinging onto the sample. The diffracted beams from the sample were collected using a high-numerical-aperture (NA) objective lens (NA = 1.2, UPLSAP 60XW, Olympus). The off-axis hologram was recorded using a CMOS image sensor (FL3-U3–13Y3MC, FLIR Systems). For 3D epifluorescence imaging, LGP120-GFP was excited using a LED light source (488 nm). Deconvolution of reconstructed 3D fluorescence images was performed using commercial software (AutoQuant X3, Media Cybernetics). The visualization of 3D RI maps and its correlative 3D fluorescence signal with green pseudocolour was performed using commercial software (TomoStudio, Tomocube).

2.12. Surface-Labelling of Bacteria. R. equi strains were grown overnight in BHI medium at 30°C. Cultures were then diluted 20-fold into fresh BHI medium containing 4 mM D-Alanine azide (Flurochem) and allowed to grow for a further 3 hours at 30°C. Bacteria were then washed twice with PBS before being resuspended in PBS containing $20\,\mu M$ FITC-Alkyne (DBCO-PEG 4-5/6-FAM; Jena Bioscience). Samples were rotated at 37°C, in the dark, for 30 min, and then washed twice with PBS before being used in infection assays.

2.13. Immunofluorescence Lysosomal Size Quantification. ImageJ (v 2.1.0/1.53c) was used to quantify lysosomal sizes. A minimum of 10 images was used per experiment, with $n > 3$. Images were acquired with a minimum of a 63X objective and a 2.5x optical zoom. Image thresholds were matched to match the immunofluorescence pattern before converting the image into an 8-bit binary image. The watershed function was applied, and the scale was set using the metadata from the image. The analyse particles function was used with size = $0.05 - 10\,\mu m^2$, excluding edges and including holes.

2.14. pH Measurements. For pH measurements, mouse macrophages were seeded at 1×10^5 cells per well of a 96-well plate. Cells were then infected with fluorescein-labelled R. equi. pH measurements were taken 24 h postinfection. Ratiometric fluorescence measurements were then undertaken by Ex = 485/14 nm and 440/12 nm with Em = 532/30 nm, using a BMG CLARIOstar. Calibration curves were generated by incubating R. equi infected cells with buffers of defined pH (4.5-7.5) with $20\,\mu M$ monensin (Sigma) and $10\,\mu M$ nigericin (Sigma) [41]. For measurement of macrophage lysosomes, cells were incubated with 1 mg/ml fluorescein-dextran (10,000 MW; Invitrogen, ThermoFisher Scientific) for 4 h and then dextran-free media for 1 h. The pH of VapA-containing compartments was undertaken by incubating cells for 20 h with $5\,\mu g/ml$ VapA-pHluorin-2 or pHluorin-2 protein and then 1 h with VapA-free medium. The pH of the VapA compartment was measured, again with ratiometric measurements, with Ex = 390/20 nm and 468.5/13 nm, and with Em = 509/16 (BMG CLARIOstar). pHluorin-2 was used to generate a calibration curve (buffers as for fluorescein). Fluorescein and pHluorin-2 calibration curves are shown in supplemental data.

2.15. SDS-PAGE and Western Blotting. Cell or lysosomal lysates were generated by incubating samples in lysis buffer (150 mM NaCl, 20 mM Tris, pH 8.0, 1 mM EDTA, 0.5% (v/v) NP-40, protease inhibitors (Roche)) and then detergent insoluble material removed by centrifugation (16,000 g 10 min). Protein in detergent-soluble material was quantified by BCA protein assay and then samples heated to 95°C for 5 min in sample buffer containing 10% (v/v) ß-mercaptoethanol (Sigma). Western blotting was undertaken as previously described [35].

3. Results

3.1. VapA, VapB, VapK, and VapN Core Regions Have a High Degree of Identity. Previously, we demonstrated that the core region of VapA alone (consisting of the β-barrel domain of VapA) was sufficient to disrupt the lysosomes [35]. When full-length Vap sequences are aligned, VapA exhibits the highest degree of identity to VapB (77%) with more modest identity of 61%, to VapK1/2 (VapK1 and K2 differ only by one amino acid) and VapN, and less than 53% for all other Vap proteins. For the predicted core regions, VapA maintains the highest identity to Vap B (86%), but the identity to VapK and VapN increases to 78% and 72%, respectively. A heat map depiction of these analyses suggested that when considering just the core regions of Vaps, VapA, VapB, VapK, and VapN may have a commonality of function (Figure 1), which would be consistent with vap gene ancestry [23].

3.2. VapA, VapB, VapK, and VapN All Induce Enlargement of Lysosomes. A good indicator of Vap function is a simple assay where purified recombinant Vaps are exogenously fed to eukaryotic cells and immunofluorescence is used to immunolabel the lysosome. The size of the lysosome can then be measured. We have shown that the core region of VapA protein can disrupt endolysosomes giving rise to swollen LGP120-positive (the rat equivalent of human LAMP1)
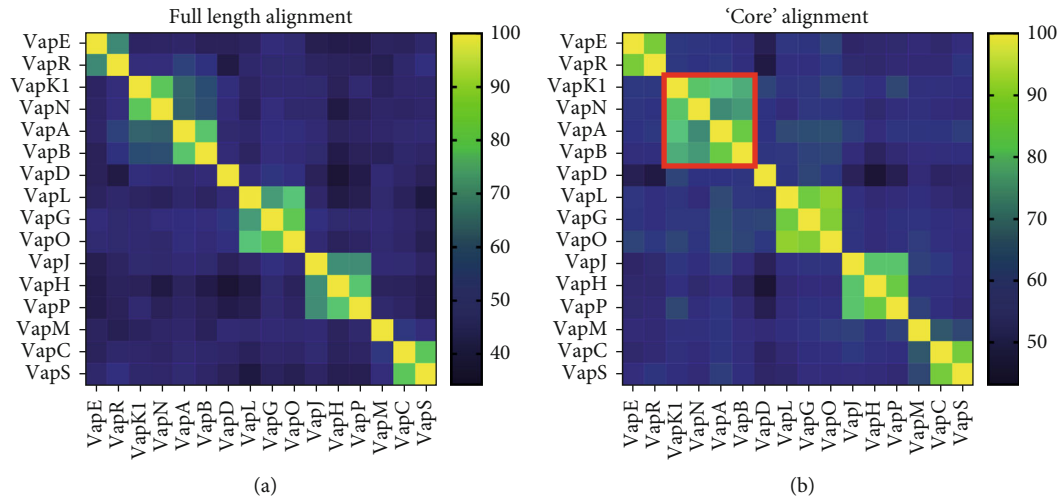
FIGURE 1: Vaps A, B, K, and N have a high degree of identity. Heat map representation of pairwise protein identities between full-length Vap proteins (a) and the β-barrel core region (b). Sequences used are in Figure S1. Red box highlights the increase in identity between Vaps A, B, K, and N compared to full-length proteins.

endolysosomes [35]. Based on the sequence identity of the core regions of Vaps, we predicted that Vaps B, K, and N would cause similar disruption to endocytic compartments. Indeed, swollen LGP120 positive structures, on average twice the diameter of normal lysosomes, were observed when the core region of Vaps B, K, and N were fed to normal rat kidney (NRK) cells (Figures 2(a) and 2(b)). In contrast, no change in the size of lysosomes was observed in cells fed with Vaps D, E, G, and L (Figures 2(a) and 2(b)). These data suggest that there is a threshold level of identity to VapA in which proteins perturb lysosomes.

3.3. LC3 Degradation in Autolysosomes Is Inhibited by VapA, VapB, VapK, and VapN. VapA disrupts endolysosomes, and we have previously observed an increase in microtubule-associated protein light chain 3 (LC3) protein in VapA-treated cells [35]. LC3 is commonly used as an autophagosome marker, and its accumulation is an indicator of autolysosomal dysfunction. When NRK cells were treated with the Vaps (A, K, N, and B) which induce lysosomal swelling (as in Figure 2), LC3 levels were found to increase when assessed by both immunofluorescence (Figure 3(a)) and western blotting (Figure 3(b)). No LC3 accumulation was observed in untreated cells or in cells that were treated with VapD (Figure 3). Relative to the control and VapD, the immunofluorescence is clear for VapA, VapB, VapK, and VapN and especially striking for A and N in this assay. Altogether, these data indicate that VapA, B, K, and N disrupt endolysosomes.

3.4. Vaps A, B, K, and N Added Exogenously Can Promote R. equi Intracellular Survival in Bacteria Lacking vapA. To further test whether Vaps B, K, and N are functionally the equivalent of VapA, mouse macrophages were infected with *R. equi* harbouring the virulence plasmid pVapA (*R. equi* strain 103+), without the virulence plasmid (*R. equi* strain 103-) or with *R. equi* 103+ lacking *vapA* (*R. equi* 103+ *ΔvapA*) [42]. Without pVapA (*R. equi* 103-), *R. equi* fails to proliferate intracellularly, and a lack of proliferation is

also observed when just vapA is deleted from the virulence plasmid (*R. equi* 103+ *ΔvapA*) (Figure 4). Macrophages were then infected with these *R. equi* strains in the presence of recombinant Vaps in the culture medium. Assessing colony forming units 24 h postinfection, *R. equi* 103+ bacterial survival was enhanced by the addition of proteins VapA (2.5-fold), B (1.25-fold), and K (1.5-fold) (Figure 4). While 103+ *ΔvapA* bacteria did not persist under normal conditions, the addition of recombinant VapA protein not only restored virulence but enhanced virulence (1.75-fold) above wild-type bacteria (*R. equi* 103+), as did the addition of VapB (1.3-fold) and VapK (1.25-fold) (Figure 4). Initially, VapN did not appear to restore virulence, but when macrophage monolayers were observed post-bacterial infection, the majority of the macrophages had detached from the culture wells. Reducing the concentrations of VapN in the experiment from 5 μg/ml to 1 μg/ml showed that VapN can aid bacterial survival (1.5-fold greater than 103+) when *vapA* is deleted (Figure 4). In addition to *vapA*, *virR* and *virS* (from the virulence plasmid) are required to confer virulence [28], and in all conditions tested, none of the recombinant Vaps could restore virulence in *R. equi* 103- strains (Figure 4). With all three *R. equi* strains, recombinant Vaps D, E, G, and L did not aid *R. equi* intracellular survival (Figure 4). In experiments similar to ours, recombinant VapK protein has previously been shown to restore virulence in a *ΔvapA* strain, but VapB did not have any effect [39]. This latter study was using VapB at 100 nM, and in our study, 5 μg/ml equates to 400 nM. When we used VapB protein at 1 μg/ml (equivalent of 82 nM), we did not see VapB being able to aid *R. equi* intracellular survival. These data suggest that VapB, VapK, and VapN can substitute for VapA in assisting *R. equi* survival, but data with VapB and VapN indicated that the ability of a Vap protein to mimic VapA in aiding *R. equi* to survive intracellularly is dosage dependent.

3.5. Vaps Have Variable Activities in Inducing Lysosomal Dysfunction. To examine whether Vaps A, B, K, and N have
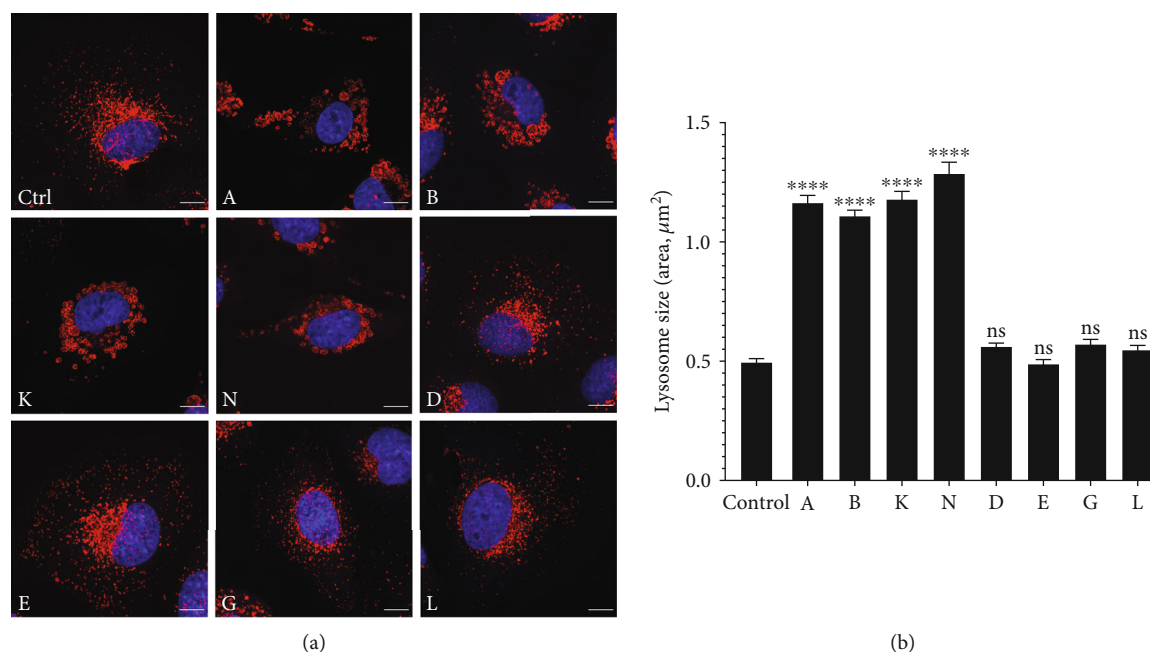
(a)

(b)

FIGURE 2: Vap-induced lysosomal swelling is not unique to VapA. (a). NRK cells were incubated without (Ctrl) or with 40 μg/ml recombinant Vaps (denoted by alphabetic character) for 20 h. Cells were fixed and the lysosomes immunolabelled with an anti-LGP120 monoclonal antibody, followed by an Alexa Fluor 555-labelled secondary antibody (red). Cell nuclei were stained with DAPI (blue). Scale bars 10 μm. (b). The size of lysosomes in the images was measured using automatic thresholding and quantification with ImageJ. Data are from 30 images in total from three separate experiments (10 images per experiment). Data are mean ± SEM ($n = 3$). ****$p < 0.001$ vs. control.
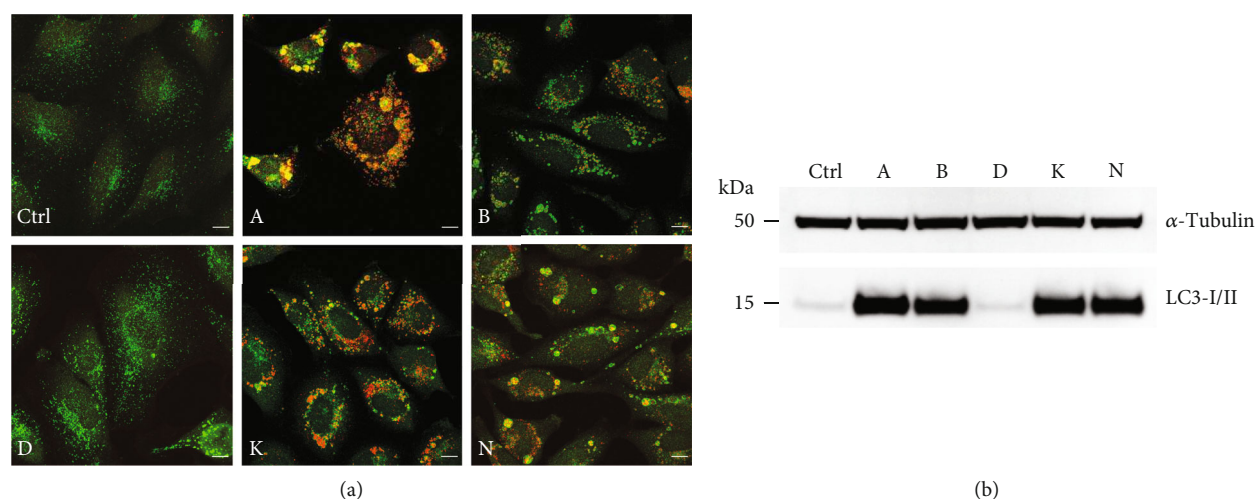

(a)

(b)

FIGURE 3: VapA, VapB, VapK, and VapN cause accumulation of LC3 in NRK cells. (a) NRK cells were incubated without (Ctrl) or with 40 μg/ml recombinant Vaps (denoted by alphabetic character) for 20 h. Cells were fixed and immunolabelled for LGP110 (green) and LC3 (red) before confocal imaging. Scale bars 10 μm. (b) NRK cells were incubated with protein as in (a) before lysing, and equal amounts of protein were immunoblotted for α-tubulin or total LC3 (I and II).

different biological activities, we revisited the lysosomal swelling assay, as depicted in Figure 2, using Vaps at a variety of concentrations (Figure 5). At 32 μg/ml, Vaps A, B, K, and N all cause lysosomal swelling to the same extent (Figure 5), as has been seen when proteins were used at 40 μg/ml (Figure 2). However, at lower protein concentrations, a hierarchy of the ability of Vaps A, B, K, and N to cause lysosomal swelling is observed, with VapN biological

activity > VapA > VapK > VapB (Figure 5). The activity seen in the lysosomal swelling assay is slightly different to the infection assay, but the latter assay is dependent upon eukaryotic cell survival. Macrophage viability was assessed in the presence of varying concentrations of Vaps. At 4 μg/ml, macrophage viability was reduced to 88%, 78%, 50%, and 60% by Vaps B, A, K, and N, respectively (Figure S2), indicating that VapK and N are detrimental to cells at quite
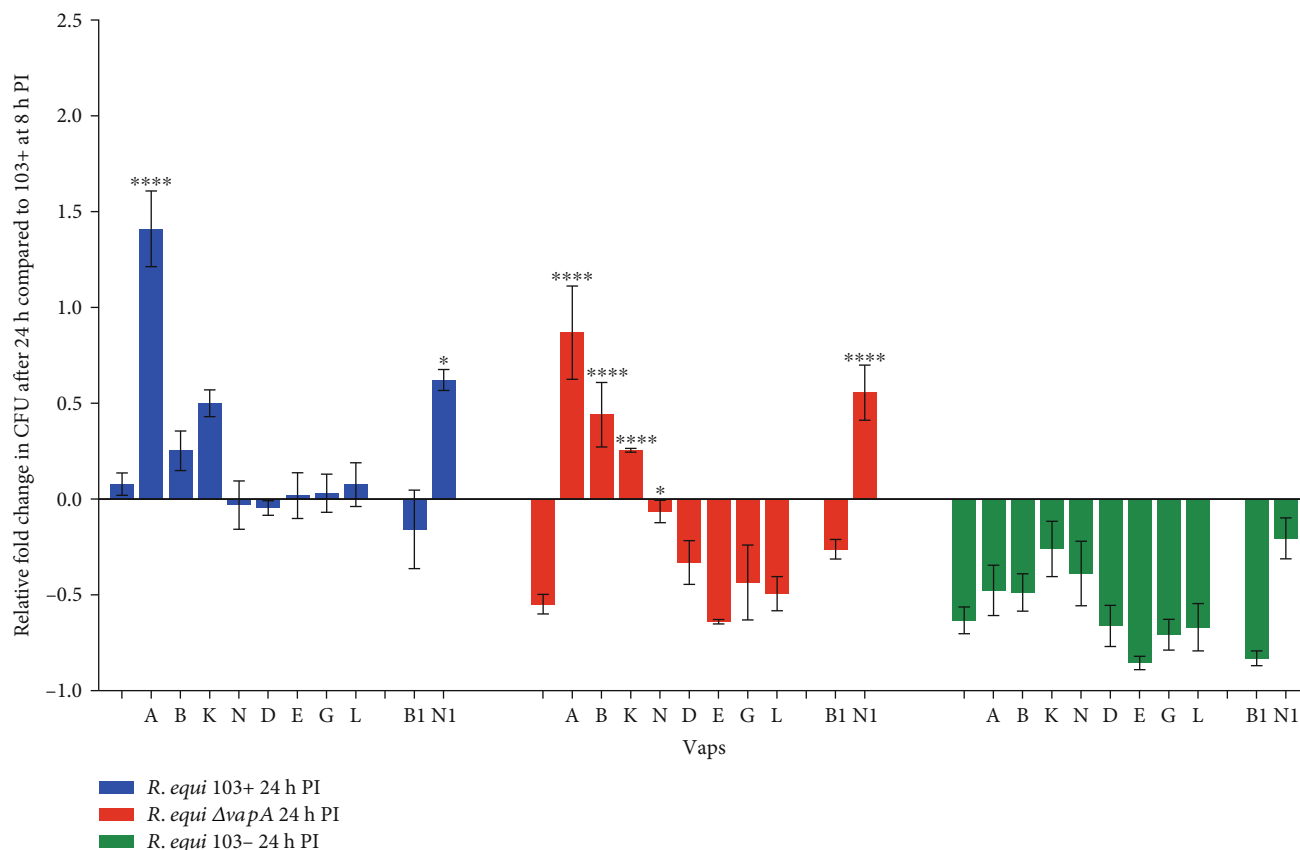
FIGURE 4: VapA, VapB, VapK, and VapN can restore virulence in ΔvapA *R. equi*. J774A.1 cells were infected with *R. equi* strains 103+ (blue), *ΔvapA* (red), or 103- (green) without or in the presence of recombinant Vaps (5 μg/ml). Cells were lysed at 8 or 24 h, and viable cfu was determined. Data shown are relative change in cfu at 24 h compared to the 103 + 8 h postinfection (PI). Data are mean ± SEM ($n \geq 3$). Statistics show Dunnett's multiple comparison tests for each *R. equi* strain compared to the no-protein sample. $^{*}p < 0.05$, $^{****}p < 0.0001$. VapB and VapN were also used at 1 μg/ml as denoted by B1 and N1, respectively.
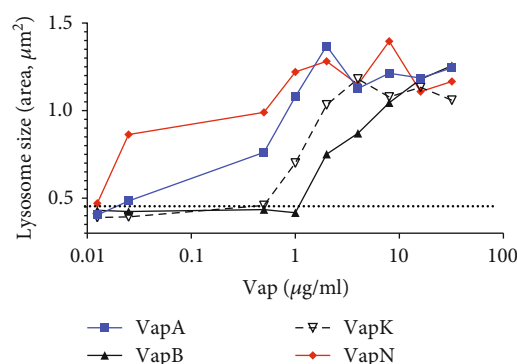

FIGURE 5: Vaps A, B, K, and N vary in their ability to promote lysosome dysfunction. NRK cells were incubated with or without varying concentrations of Vaps A, B, K, and N for 24 h. Cells were fixed and the lysosomes immunolabelled with an anti-LGP120 monoclonal antibody, followed by an Alexa Fluor 555-labelled secondary antibody. The lysosome sizes of images were quantified using automatic thresholding and quantification with ImageJ. Data are from the analyses of 10 images per condition ($n = 1$). Control lysosomal size is indicated by the dashed horizontal line.

modest levels. Macrophage viability, therefore, affects the infection assay and explains why VapA and VapB, which do not have a major effect on macrophage viability, are seen to have more significant effects in promoting *R. equi* survival and why a lower concentration of VapN protein was required in the infection assay to observe *R. equi* proliferation.

3.6. VapA Reduces the Acidity of the Phagolysosome. We previously stated that VapA could swell lysosomal compartments and that these swollen compartments were acidic, as assessed by using LysoTracker [35]. These data differed from observations with virulent *R. equi*, which were determined to be in nonacidic compartments [36]. Lysosomes are made acidic by the action of an ATPase-dependent proton pump, the vacuolar-type ATPase (V-ATPase), which consists of two multi-subunit complexes, the membrane-associated V_0 domain and the peripherally associated V_1 domain. Recently, it has been suggested that VapA prevents incorporation of the V-ATPase (at least the E-subunit of the V_1 domain when overexpressed) into the phagolysosomal compartment and that proton leakage (by membrane permeabilisation) increases phagolysosomal pH, and this aids *R. equi* survival [37]. Our earlier LysoTracker data may be explained by the use of different cell types and the observations that the pH of lysosomes

can vary depending upon the location of the lysosome within the cell [43]. Moreover, in some cell types, terminal storage lysosomes may not be acidic [44]. While LysoTracker accumulates in compartments where the pH < 6.5, it is not sensitive to small changes in pH and, therefore, does not report the precise lysosomal pH [45]. Furthermore, measurements of intracellular pH using fluid-phase reporter probes may run the risk of the probes localising to a compartment other than that occupied by the phagocytosed bacterium, particularly if the late endocytic compartment has been perturbed, as is the case when using VapA. Hence, to directly measure the pH of the *R. equi*-containing phagosomal compartment, we utilised metabolic labelling and bioorthogonal click-chemistry and grew *R. equi* strains in the presence of D-alanine azide and then surface labelled the cell wall using dibenzocyclooctyne (DBCO)-fluorescein. Fluorescein is pH sensitive, and using dual-wavelength ratiometric fluorescence measurements [41], we were able to measure the pH of the phagosomal compartment surrounding *R. equi* bacteria. *R. equi* strains grown in the presence of D-alanine azide have the same growth kinetics as strains grown in normal growth medium (data not shown) and exhibit unaltered replicative characteristics in mouse macrophages (Figure 6(a)). The pH of the phagosomal compartment was measured in the *R. equi* strains 103-, 103+, and 103+ $\Delta vapA$. Nonreplicative *R. equi* (103-) were found in a phagosomal compartment of pH 5.7 (Figure 6(b)). This is very similar to the pH of macrophage lysosomes measured with a fluorescein-dextran probe (pH 5.6; Figure 6(b)). By contrast, *R. equi* (103+) harbouring the intact virulence plasmid were found in a less acidic environment (pH 6.6; Figure 6(b)). *R. equi* 103+ $\Delta vapA$ were found in a compartment with a pH of 6.1, which was significantly different from that of 103+ strains but not that of 103- strains. When macrophages were fed VapA-pHluorin-2 (a pH-sensitive probe which, like fluorescein, can be excited at two wavelengths) [46], lysosomal pH was determined to be 7.1. These data validate previous studies indicating that *R. equi*-secreted VapA can neutralise the pH of the endolysosomal compartment [37].

To examine whether the pH of lysosomal compartments can be neutralised by paralogous Vap proteins, we analysed LysoTracker accumulation and fluorescence in cells incubated with other Vaps, using flow cytometry. Using mouse macrophages and Vaps at 5 μg/ml, cells were gated for live (DAPI exclusion) and single cells (Figure 6(c)), and LysoTracker fluorescence was measured (Figure 6(d)). There was a 185-fold increase in the fluorescence signal compared to control cells that had not been incubated with LysoTracker (Figure 6(e)). The V-ATPase inhibitor bafilomycin-A_1 reduced the fluorescence signal to 3-fold above control cells (Figure 6(e)). Statistically, there was no difference in the LysoTracker fluorescence between the bafilomycin-A_1 treated cells and cells incubated with Vaps A, K, and N (Figures 6(d) and 6(e)). VapB did reduce the accumulation of LysoTracker compared to control LysoTracker cells (2.3 fold reduction), but not to the same extent as VapA, K, and N. VapN showed the greatest reduction in LysoTracker accumulation in cells, then VapK, then VapA, and then VapB. The loss of acidity is not due to cells being incubated with extracellular protein, since VapL

(which has no observed effects on lysosomes) did not have any effects on the LysoTracker assay (Figures 6(d) and 6(e)). Together, these data indicate that VapA directly reduces the acidity of phagolysosomes, and this biological activity is also conferred by VapN, VapK, and, to a lesser extent, VapB.

To address whether the reduction in acidity is due to the loss of V-ATPase subunits from the VapA-positive compartment, macrophages were fed VapA or infected with *R. equi* strains (103- or 103+), and immunofluorescence was used to examine the location of V-ATPase subunits. Neither of the V-ATPase subunits ATP6V$_0$d or ATP6V$_1$D could be observed to be excluded from lysosomal membranes or *R. equi* containing phagosomes (Figure 7(a)). We then used a colloidal-iron dextran to purify lysosomes [40] from macrophages that had been incubated in the presence or absence of VapA. When analysing the purified lysosomes, from both conditions, there was an enrichment of LAMP1 and various subunits of the V-ATPase V$_0$ and V$_1$ complexes compared to the postnuclear supernatants (PNS), including ATP6V$_1$E which had been reported to be excluded by VapA [37] (Figure 7(b)). Additionally, we indirectly measured the V-ATPase activity in intact lysosomes (-/+ VapA) using a general ATPase assay and attributing V-ATPase specific activity to the proportion of the ATPase activity which was inhibited by the V-ATPase inhibitor concanamycin-A. In the presence of VapA, there was no change in the proportion of ATPase activity which could be inhibited by concanamycin-A (Figure 7(c)). Together, our data indicate that VapA does not have a direct effect on the recruitment of V-ATPase subunits (of the antibodies that we could test) to the lysosome or V-ATPase activity.

3.7. Vap Disruption of Lysosomal Acidity Correlates with Disruption to Lysosomal Hydrolase Activity. With a loss of acidic compartments, we expected that there would be a concomitant loss of lysosomal hydrolase activity. Indeed, using a similar flow cytometry gating strategy as shown in Figure 6, macrophages were incubated with Vaps and then DQ-BSA (dye-quenched bovine serum albumin) before being analysed by flow cytometry. DQ-BSA is highly fluorescently labelled, and the fluorescence is quenched. Upon endocytosis and delivery to endolysosomes, digestion of the BSA occurs, and there is an increase in fluorescence as dequenching occurs. Thus, fluorescence is an indicator of proteolytic activity. When macrophages were incubated with DQ-BSA, there was a 23-fold increase in fluorescence compared to cells which had not been incubated with DQ-BSA cells (Figured 8(a) and 8(b)). The fluorescence in control cells was reduced by 20-fold when cells were incubated with bafilomycin-A_1, indicating that hydrolase activity is pH dependent (Figures 8(a) and 8(b)). Similarly, when macrophages were fed Vaps A, B, K, or N, there was a loss of the fluorescent signal indicating a lack of DQ-BSA digestion (Figures 8(a) and 8(b)). The DQ-BSA data very much matched the LysoTracker data, with the effect of VapB being more modest compared to Vap A, K, and N and no effect with VapL. These data show that Vaps secreted from *R. equi* enable *R. equi* to survive longer in the phagolysosome by disrupting acidity and, thus, the activity of hydrolases.
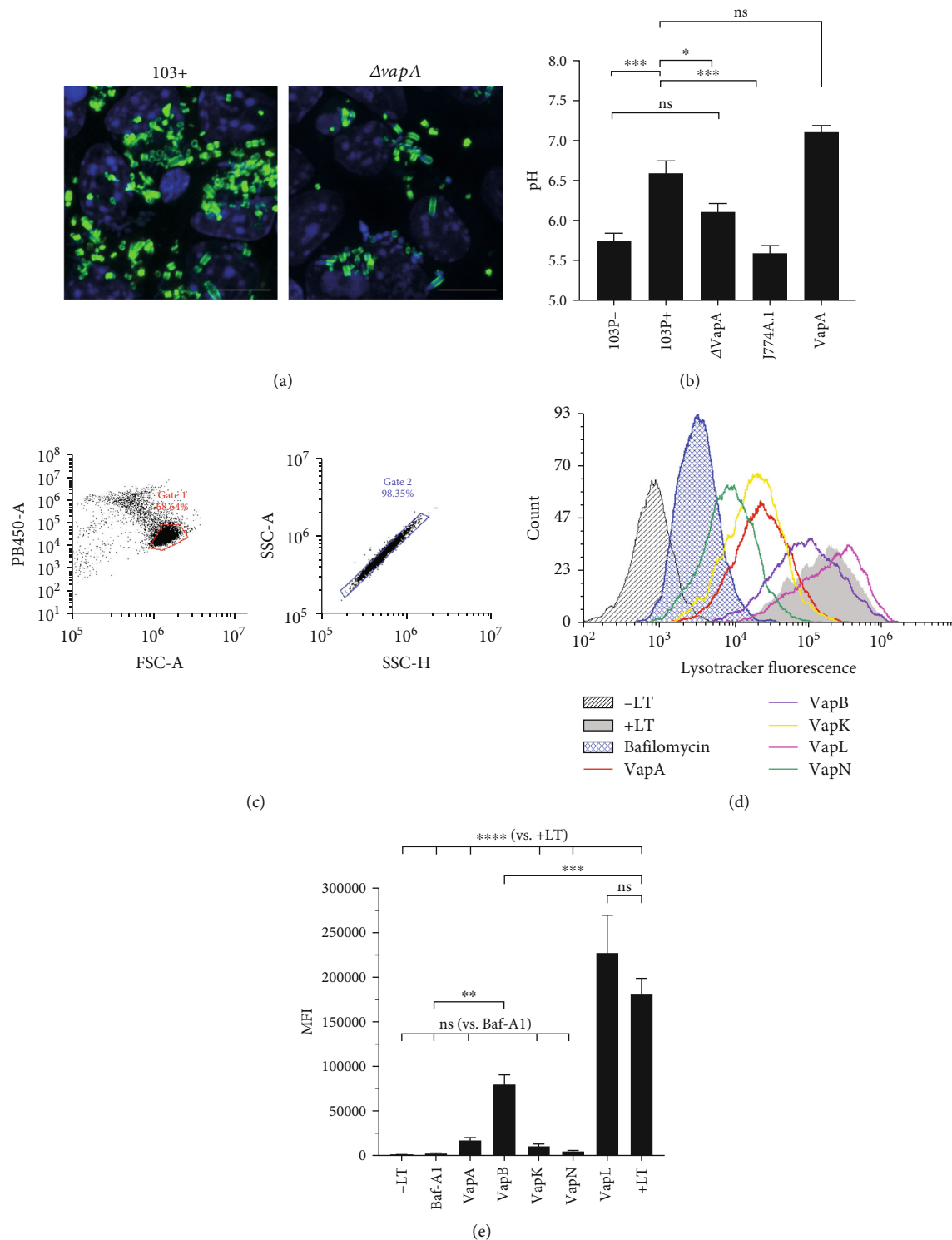
(a)

(b)

(c)

(d)

(e)

FIGURE 6: Lysosomal acidity is reduced by Vaps A, B, K, and N. (a) Fluorescent images of macrophages infected with fluorescent-peptidoglycan R. equi strains 103+ or 103+ (ΔvapA). Peptidoglycan is in green and DNA is in blue. Scale bars 10 μm. (b) Quantitative pH measurements of R.equi-containing phagosomes using fluorescein-labelled bacteria. Lysosomal pH was measured using fluorescein-labelled dextran, and VapA-positive compartments were measured using VapA-pHluorin2. Fluorescein and pHluorin2 calibration curves are shown in Figure S3. Data are mean ± SEM ($n \geq 3$). $^*p < 0.05$, $^{***}p < 0.001$. (c) Flow cytometry gating strategy used to select live cells based on DAPI exclusion (left plot; y-axis = DAPI fluorescence; x-axis = forward light scatter) and single cells (right plot; y-axis is light scattering based on cell area; x-axis is light scattering based on cell height). (d) Representative flow cytometry overlay histogram of LysoTracker (LT) fluorescence in cells treated with or without Vaps and bafilomycin-A$_1$ (Bafilomycin). 5,000 cells were counted for each condition. (e) Quantification of LysoTracker fluorescence in cells as shown in (d). Data are mean median fluorescence intensity (MFI) ± SEM ($n \geq 3$). $^{**}p < 0.01$, $^{***}p < 0.001$, $^{****}p < 0.0001$.
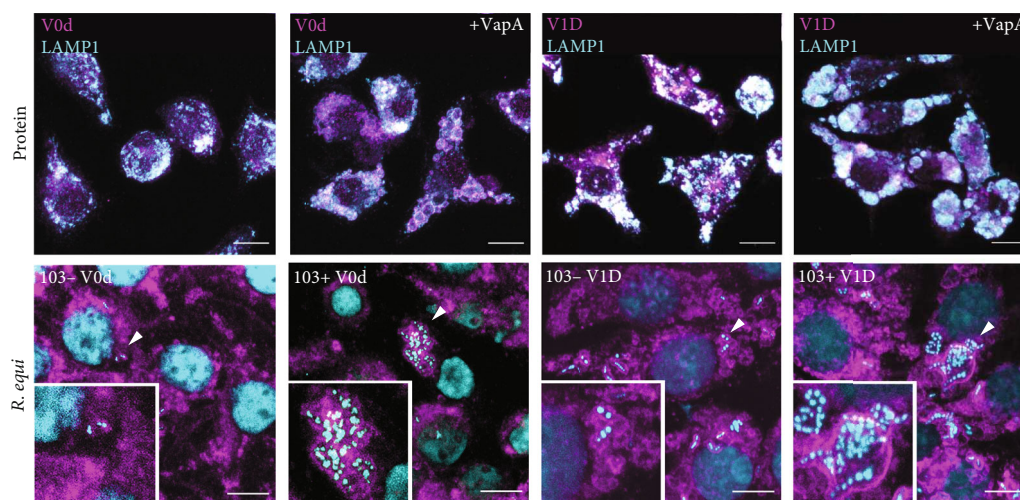
(a)
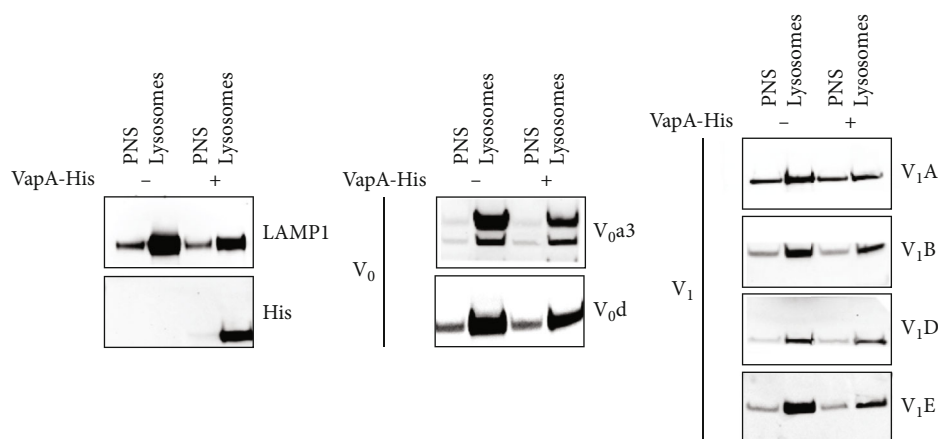
(b)
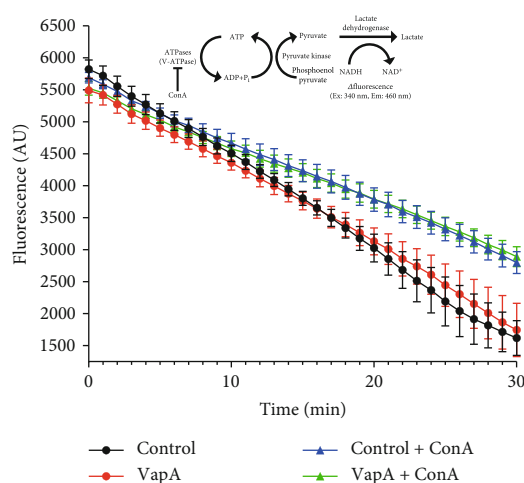
(c)

FIGURE 7: V-ATPase recruitment and activity to VapA-positive compartments is unaffected by VapA. (a) Top panels: immunofluorescence of macrophages fed -/+ VapA and immunolabelled for lysosomal-associated membrane protein-1 (LAMP-1) (cyan) or ATP6 subunits (magenta). Bottom panels: immunofluorescence of macrophages infected with 103- and 103+ *R. equi* and immunolabelled for ATP6 subunits (magenta) and DNA stained with DAPI (cyan). Scale bars = 10 μm. Arrows indicate regions used for magnification in the insets. (b). Western blotting postnuclear supernatants (PNS) and isolated lysosomes after incubation +/- VapA-His for LAMP1, His$_6$-tag, and ATP6 subunits. (c). Measurement of ATPase activity in isolated lysosomes (as in (b)) ± luminal VapA using an ATP/NADH coupled-enzyme assay (schematic shown). ATPase activity specific to the V-ATPase is inhibited by concanamycin-A (ConA). Data are mean fluorescence ± SEM ($n = 3$).

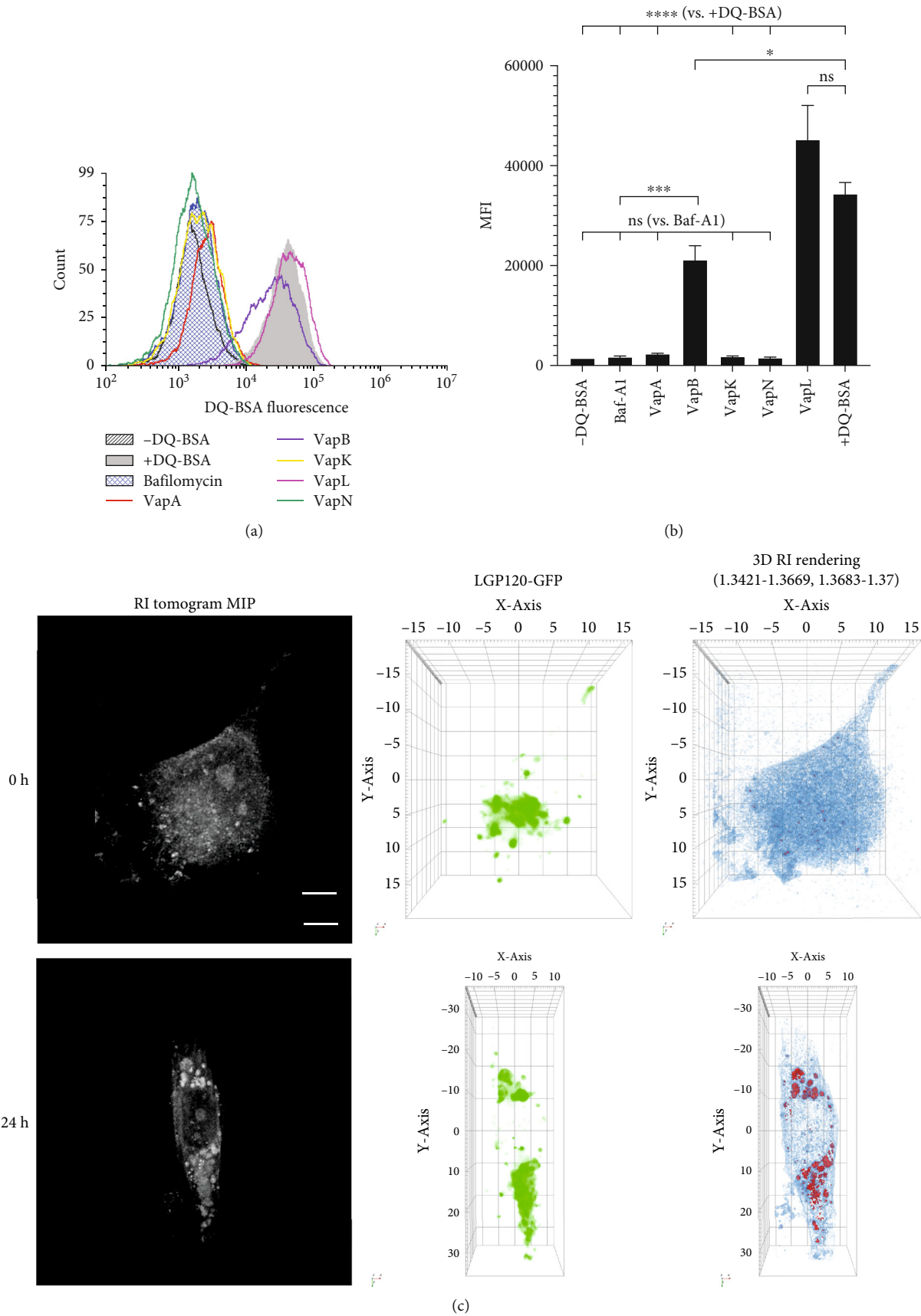(a)
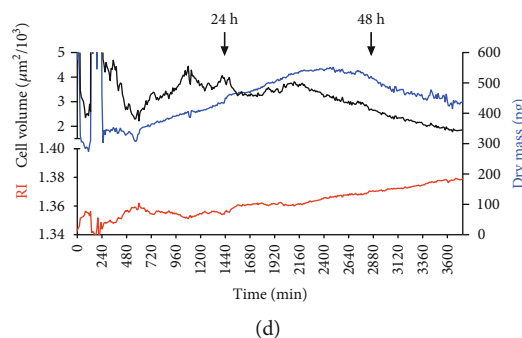

(b)

(c)

FIGURE 8: Continued.

(d)

FIGURE 8: Vaps A, B, K, and N reduce lysosomal proteolytic activity resulting in swollen compartments containing undigested material. (a) Representative flow cytometry overlay histogram of DQ-BSA fluorescence in cells treated with or without Vaps and bafilomycin-A$_1$. 5,000 cells were counted for each condition. (b) Quantification of DQ-BSA fluorescence in cells as shown in (a). Data are mean median fluorescence intensity (MFI) ± SEM ($n = 3$). $^{**}p < 0.01$, $^{***}p < 0.001$, $^{****}p < 0.0001$. (c) Holotomography of lysosomal glycoprotein-120-GFP (LGP120-GFP) Normal Rat Kidney (NRK) cell treated with VapA. Images were acquired every 10 min, and images shown represent the 0 h and 24 h images posttreatment. Refractive index (R.I.) tomographs (left panels), GFP fluorescence (middle panels), and refractive index rendering into low-density (blue) and high-density (red) regions (right panels). (d) Quantification of holotomography data (for 60 h) from the cell shown in (c). Data shown indicate the cell volume, dry mass, and overall R.I. of the cell.

We then applied holotomography to cells which have been incubated with VapA. Holotomography measures the refractive indices of samples and offers a means to probe, noninvasively and quantitatively, the structural and chemical information of cells, including morphology, membrane dynamics, and dry mass of the cell [47]. The refractive index can be correlated to density. Over 24 h, LAMP-1-GFP positive NRK cells were imaged in the presence of VapA (Figure 8(c)). At 0 h, the GFP signal did not correlate with any particular density compared to the surrounding cell, but 24 h post-VapA addition to the cells, the swollen LAMP1-GFP compartments correlated with areas of increased density (Figure 8(c)). As lysosomal density increased, there was an overall increase in cellular volume and dry mass (Figure 8(d)). At 48 h, the cell begins to lose mass as the cell begins to apoptose (Figure 8(d)). Live-cell imaging of LAMP1-GFP cells shows that VapA-swollen LAMP1 compartments remain fusogenic at least 9 h post-VapA addition (Figure S4, Movie S1). Together, these data, along with the accumulation of LC3 (Figure 3), indicate that VapA reduces the acidity of late endocytic compartments, and there is a reduction in proteolytic activity, thereby causing an accumulation of undigested material. The endolysosomes are still fusogenic (Movie S1), and in NRK cells, material from endocytic and autophagy pathways continues to be delivered to the lysosomal compartment up to 36 h after the addition of VapA, as evidenced by the increase in cell dry mass (Figure 8(c)). The loss of endolysosomal acidity and proteolytic activity is also observed with Vaps N and K, and to a lesser extent Vap B.

4. Discussion

All these data indicate that there is a good correlation between the ability of certain Vaps to disrupt late endocytic pathway acidity, reduce lysosomal proteolytic activity, and then accumulate undigested material resulting in large endolysosomes which fail to condense and reform terminal lysosomes. While R. equi may be adapted to survive short term

in a phagolysosomal environment [48], bacterial replication will be dependent upon the reduction of hydrolase activity. Our data show that in an environment with VapA-induced alkalynisation of the compartment, the compartment remains fusogenic, thereby maintaining the delivery of nutrients to the phagolysosomal compartment that can be utilised by R. equi.

The ability of any individual Vap to promote R. equi survival will be dependent upon its expression levels from the various virulence plasmids, and while VapB may not be as "potent" as VapA or VapN when compared side by side, pVAPB harbours vapB, vapK1, and vapK2 all of which can produce Vaps to disrupt endolysosomal function. Indeed, vapK1 and vapK2 are required for optimal growth of R. equi strains carrying a pVAPB plasmid and can complement growth-attenuated ΔvapA strains [30]. Together, our data indicate that vapN in pVAPN is the equivalent of vapA in pVAPA, and vapB, vapK1, and vapK2 in pVAPB can all contribute to R. equi survival. In R. equi pVAPB strains, vapK1 and vapK2 are likely to be more critical than vapB in promoting intracellular survival. While distinct virulence plasmids may be associated with particular animal sources, the plasmid type (pVAPA, pVAPB, and pVAPN) does not determine the ability of R. equi to replicate inside a particular species host cell [25], and thus, any plasmid which expresses VapA or an equivalent protein such as VapK or VapN is of importance.

Importantly, VapA, K and N, and, to a certain extent, VapB all appear to have the same mechanism of action, in that they reduce late endocytic acidity and lysosomal hydrolase activity. This appears to contradict recent data reporting that VapN did not alter lysosomal hydrolase activity [38]. This might be explained by differing flow cytometry analyses. In the earlier study, scatter alone was used to assess viability in the presence of 50 μg/ml Vap proteins. In our hands, this protocol led to cell death in approximately 60% of the mouse macrophages. Additionally, while we had previously shown that the N-terminal region of VapA is not critical for VapA function [35], we have not evaluated whether the N-terminal regions in other Vap-proteins provide a

regulatory function. The more recent study by Hansen et al. [38] used full-length proteins (without the signal sequence), whereas our study here has only used the β-barrel core region.

It has been demonstrated that VapA binds to phosphatidic acid [39] and can permeabilise artificial membranes allowing for proton leakage [37]. However, VapB bound phosphatidic acid weakly, and VapK not at all [39]. Since we find VapA has similar lysosomal disruptive properties to VapK, and VapB has limited lysosomal disruptive properties, the binding of VapA to phosphatidic acid may be an artefactual property of VapA. The modest permeabilisation of liposomes with VapA [48] is not recapitulated to the same extent with VapB or VapN, suggesting that this observation may also be an effect which is unrelated to the true biological activity of VapA. Furthermore, VapA is found primarily localising to intracellular membranes [37] and not the phagolysosomal limiting membrane (which we also see in Figure S5), and so it is unclear how membrane permeabilisation would occur if VapA is bound to lumenal-vesicular membranes.

The lysosomal pH gradient is generated by the action of a V-type ATPase (V-ATPase) which uses ATP to pump protons into the lysosomal lumen. The movement of protons would create a membrane potential which would restrain the activity of the V-ATPase if left uncompensated [49]. Thus, there is a counterion conductance pathway which neutralises the charge imbalance. The counterion conductance pathway may be satisfied by the influx of cytosolic anions such as Cl⁻ into the lysosome [50, 51], Cl⁻/H⁺ exchangers such as ClC-7 [52], or efflux of cations [53, 54]. The role of Cl⁻ in maintaining lysosomal pH by complementing the V-ATPase is controversial [51–53], and more recent research has demonstrated that ClC-7 does not contribute to lysosomal pH, but instead, Cl⁻ is used to activate lumenal hydrolases [55]. It is interesting to speculate that if VapA was to disrupt Cl⁻ entry, then potentially, this could either disrupt the activity of the V-ATPase (if Cl⁻ is acting as a counterion) or lead to a loss of hydrolase activity, causing undigested material to accumulate and lysosomal size to increase. A doubling of lysosomal diameter equates to an 8-fold increase in volume which could then account for changes seen in lumenal pH if the number of H⁺ ions remains the same.

In addition to Cl⁻/H⁺ exchangers, lysosomes continually leak H⁺ equivalents. Proton leakage can occur in many ways including the cotransport with organic solutes such as amino acids [56, 57] or through a proton-activated proton channel such as TMEM175 [58, 59]. If the V-ATPase is not directly inhibited by VapA (our study here and [37]), then there has to be a change in the concentration of protons in the lysosomal lumen to account for the observed change in pH. VapA may permeabilise the membrane, but as mentioned, this is seen to a much lesser extent with VapB or VapN [38], whereas in our study, VapN has the highest lysosomal alkalinisation activity. VapA could accelerate proton-coupled solute export, though the removal of useable solutes to a phagosomal-membrane contained R. equi might be disadvantageous to the bacterium. VapA may accelerate proton leak through a channel such as TMEM175. Alternatively, VapA may change one of the numerous ion or solute channels in such a way as to alter the osmolarity of the lysosome, creating an increase in volume, which as mentioned would reduce the proton concentration and reduce acidity. It, therefore, remains to be seen as to how, mechanistically, VapA disrupts the proton gradient in phagolysosomes, but our study demonstrates that any biological activity of VapA should also be observed in VapN and VapK, which will help eliminate potential spurious observations.

To date, while most research has concentrated on the role of VapA in promoting R. equi virulence, our study here demonstrates that VapK and VapN have the same lysosomal disrupting ability. R. equi only needs to produce one of these proteins to aid in its intracellular survival, and thus, VapA should not be the sole focus in understanding how lysosomes are disrupted. Given the emergence of antibiotic-resistant R. equi, a biologic that can disrupt Vap A, K, and N functions is likely to prove useful in treating R. equi infections. Since Vap A, K, and N appear to work mechanistically in the same manner, then a single therapeutic to VapA, K, or N should be beneficial in treating an R. equi infection independent of the virulence plasmid harboured.

Data Availability

Data for this study is available from the corresponding author upon request.

Disclosure

Timothy R. Ganderton's current address is Centre de Ressources Biologique, Hôpital Lariboisière, 75475 Paris, France.

Conflicts of Interest

The authors declare that there is no conflict of interest regarding the publication of this paper.

Supplementary Materials

Supplementary data includes details of the protein sequences used in the study (S1), the effects of Vaps on eukaryotic cell apoptosis (S2), pH calibration curves for pH measurements (S3), a movie (Movie S1, and Figure S4) and a joint-deconvolution image of VapA in a swollen lysosomal compartment (S5). (Supplementary Materials)

References

[1] J. A. Vázquez-Boland, S. Giguère, A. Hapeshi, I. MacArthur, E. Anastasi, and A. Valero-Rello, "*Rhodococcus equi*: the many facets of a pathogenic actinomycete," *Veterinary Microbiology*, vol. 167, no. 1-2, pp. 9–33, 2013.

[2] M. Żychska, L. Witkowski, A. Klementowska et al., "*Rhodococcus equi*-occurrence in goats and clinical case report," *Pathogens*, vol. 10, no. 9, p. 1141, 2021.

[3] R. Sting, I. Schwabe, M. Kieferle, M. Münch, and J. Rau, "Fatal infection in an alpaca (*Vicugna pacos*) caused by pathogenic *Rhodococcus equi*," *Animals*, vol. 12, no. 10, p. 1303, 2022.

[4] J. F. Prescott, "*Rhodococcus equi*: an animal and human pathogen," *Clinical Microbiology Reviews*, vol. 4, no. 1, pp. 20–34, 1991.

[5] G. Muscatello, D. P. Leadon, M. Klay et al., "*Rhodococcus equi* infection in foals: the science of 'rattles'," *Equine Veterinary Journal*, vol. 39, pp. 470–478, 2007.

[6] S. Giguère, N. D. Cohen, M. Keith Chaffin et al., "Diagnosis, treatment, control, and prevention of infections caused by *Rhodococcus equi* in foals," *Journal of Veterinary Internal Medicine*, vol. 25, no. 6, pp. 1209–1220, 2011.

[7] A. J. Burton, S. Giguère, T. L. Sturgill et al., "Macrolide- and rifampin-resistant *Rhodococcus equi* on a horse breeding farm, Kentucky, USA," *Emerging Infectious Diseases*, vol. 19, no. 2, pp. 282–285, 2013.

[8] S. Giguère, E. Lee, E. Williams et al., "Determination of the prevalence of antimicrobial resistance to macrolide antimicrobials or rifampin in *Rhodococcus equi* isolates and treatment outcome in foals infected with antimicrobial-resistant isolates of R equi," *Journal of the American Veterinary Medical Association*, vol. 237, no. 1, pp. 74–81, 2010.

[9] L. Huber, S. Giguère, N. D. Cohen et al., "Prevalence and risk factors associated with emergence of *Rhodococcus equi* resistance to macrolides and rifampicin in horse-breeding farms in Kentucky, USA," *Veterinary Microbiology*, vol. 235, pp. 243–247, 2019.

[10] S. Álvarez-Narváez, S. Giguère, N. Cohen, N. Slovis, and J. A. Vázquez-Boland, "Spread of multidrug-resistant *Rhodococcus equi*, United States," *Emerging Infectious Diseases*, vol. 27, no. 2, pp. 529–537, 2021.

[11] C. Higgins and L. Huber, "*Rhodococcus equi*: challenges to treat infections and to mitigate antimicrobial resistance," *Journal of Equine Veterinary Science*, vol. 127, article 104845, 2023.

[12] S. Topino, V. Galati, E. Grilli, and N. Petrosillo, "*Rhodococcus equi* infection in HIV-infected individuals: case reports and review of the literature," *AIDS Patient Care and STDs*, vol. 24, no. 4, pp. 211–222, 2010.

[13] S. R. Nath, A. P. Mathew, A. Mohan, and K. R. Anila, "*Rhodococcus equi* granulomatous mastitis in an immunocompetent patient," *Journal of Medical Microbiology*, vol. 62, no. 8, pp. 1253–1255, 2013.

[14] M. Y. Khan, S. Ali, and S. Baqi, "*Rhodococcus equi* pneumonia in a live related renal transplant recipient," *The Journal of the Pakistan Medical Association*, vol. 63, no. 5, pp. 635–638, 2013.

[15] P. Di Carlo, L. Pipitò, E. Orlando et al., "Intestinal lesions due to *Rhodococcus equi* in a patient with advanced retroviral disease and pulmonary infection: a case of colonic malakoplakia," *Cureus*, vol. 15, no. 7, article e42248, 2023.

[16] S. H. de Carvalho, R. M. Pereira Lopes, E. G. Kroon, I. V. da Silva Teixeira, and N. L. Caetano Corrêa, "Maldi-Tof-Ms identified Rhodococcus hoagie bacteraemia in an immunocompromised patient," *Journal of Ayub Medical College, Abbottabad: JAMC*, vol. 35, no. 2, pp. 337–340, 2023.

[17] A. Lührmann, N. Mauder, T. Sydor et al., "Necrotic death of *Rhodococcus equi*-infected macrophages is regulated by virulence-associated plasmids," *Infection and Immunity*, vol. 72, no. 2, pp. 853–862, 2004.

[18] R. Wada, M. Kamada, T. Anzai et al., "Pathogenicity and virulence of *Rhodococcus equi* in foals following intratracheal challenge," *Veterinary Microbiology*, vol. 56, no. 3-4, pp. 301–312, 1997.

[19] S. Giguère, M. K. Hondalus, J. A. Yager, P. Darrah, D. M. Mosser, and J. F. Prescott, "Role of the 85-kilobase plasmid and plasmid-encoded virulence-associated protein a in intracellular survival and virulence of *Rhodococcus equi*," *Infection and Immunity*, vol. 67, no. 7, pp. 3548–3557, 1999.

[20] S. Takai, H. Madarame, C. Matsumoto et al., "Pathogenesis of *Rhodococcus equi* infection in mice: roles of virulence plasmids and granulomagenic activity of bacteria," *FEMS Immunology and Medical Microbiology*, vol. 11, no. 3, pp. 181–190, 1995.

[21] M. K. Hondalus and D. M. Mosser, "Survival and replication of *Rhodococcus equi* in macrophages," *Infection and Immunity*, vol. 62, no. 10, pp. 4167–4175, 1994.

[22] S. Takai, Y. Watanabe, T. Ikeda et al., "Virulence-associated plasmids in *Rhodococcus equi*," *Journal of Clinical Microbiology*, vol. 31, no. 7, pp. 1726–1729, 1993.

[23] M. Letek, A. A. Ocampo-Sosa, M. Sanders et al., "Evolution of the *Rhodococcus equi* vap pathogenicity island seen through comparison of host-associated vapA and vapB virulence plasmids," *Journal of Bacteriology*, vol. 190, no. 17, pp. 5797–5805, 2008.

[24] A. Valero-Rello, A. Hapeshi, E. Anastasi et al., "An invertron-like linear plasmid mediates intracellular survival and virulence in bovine isolates of *Rhodococcus equi*," *Infection and Immunity*, vol. 83, no. 7, pp. 2725–2737, 2015.

[25] J. M. Willingham-Lane, L. J. Berghaus, S. Giguère, and M. K. Hondalus, "Influence of plasmid type on the replication of *Rhodococcus equi* in host macrophages," *mSphere*, vol. 1, no. 5, p. 1, 2016.

[26] S. Takai, T. Sekizaki, T. Ozawa, T. Sugawara, Y. Watanabe, and S. Tsubaki, "Association between a large plasmid and 15- to 17-kilodalton antigens in virulent *Rhodococcus equi*," *Infection and Immunity*, vol. 59, no. 11, pp. 4056–4060, 1991.

[27] S. Jain, B. R. Bloom, and M. K. Hondalus, "Deletion of vapA encoding virulence associated protein a attenuates the intracellular actinomycete *Rhodococcus equi*," *Molecular Microbiology*, vol. 50, no. 1, pp. 115–128, 2003.

[28] G. B. Coulson, A. A. Miranda-CasoLuengo, R. Miranda-Caso-Luengo et al., "Transcriptome reprogramming by plasmid-encoded transcriptional regulators is required for host niche adaption of a macrophage pathogen," *Infection and Immunity*, vol. 83, no. 8, pp. 3137–3145, 2015.

[29] J. Ren and J. F. Prescott, "The effect of mutation on *Rhodococcus equi* virulence plasmid gene expression and mouse virulence," *Veterinary Microbiology*, vol. 103, no. 3-4, pp. 219–230, 2004.

[30] J. M. Willingham-Lane, G. B. Coulson, and M. K. Hondalus, "Identification of a VapA virulence factor functional homolog in *Rhodococcus equi* isolates housing the pVAPB plasmid," *PLoS One*, vol. 13, no. 10, article e0204475, 2018.

[31] C. Geerds, J. Wohlmann, A. Haas, and H. H. Niemann, "Structure of *Rhodococcus equi* virulence-associated protein B (VapB) reveals an eight-stranded antiparallel β-barrel consisting of two Greek-key motifs," *Acta Crystallographica. Section F, Structural Biology and Crystallization Communications*, vol. 70, no. 7, pp. 866–871, 2014.

[32] J. L. Whittingham, E. V. Blagova, C. E. Finn et al., "Structure of the virulence-associated protein VapD from the intracellular pathogen *Rhodococcus equi*," *Acta Crystallographica. Section*

D, Biological Crystallography, vol. 70, no. 8, pp. 2139–2151, 2014.

[33] T. Okoko, E. V. Blagova, J. L. Whittingham, L. G. Dover, and A. J. Wilkinson, "Structural characterisation of the virulence-associated protein VapG from the horse pathogen *Rhodococcus equi*," *Veterinary Microbiology*, vol. 179, no. 1-2, pp. 42–52, 2015.

[34] J. Jumper, R. Evans, A. Pritzel et al., "Highly accurate protein structure prediction with AlphaFold," *Nature*, vol. 596, no. 7873, pp. 583–589, 2021.

[35] A. P. Rofe, L. J. Davis, J. L. Whittingham, E. C. Latimer-Bowman, A. J. Wilkinson, and P. R. Pryor, "The *Rhodococcus equi* virulence protein VapA disrupts endolysosome function and stimulates lysosome biogenesis," *Microbiology*, vol. 6, no. 2, 2017.

[36] K. Toyooka, S. Takai, and T. Kirikae, "*Rhodococcus equi* can survive a phagolysosomal environment in macrophages by suppressing acidification of the phagolysosome," *Journal of Medical Microbiology*, vol. 54, no. 11, pp. 1007–1015, 2005.

[37] K. von Bargen, M. Scraba, I. Krämer et al., "Virulence-associated protein a fromRhodococcus equiis an intercompartmental pH-neutralising virulence factor," *Cellular Microbiology*, vol. 21, no. 1, Article ID e12958, 2019.

[38] P. Hansen, T. Haubenthal, C. Reiter et al., "Differential effects of *Rhodococcus equi* virulence-associated proteins on macrophages and artificial lipid membranes," *Microbiology Spectrum*, vol. 11, no. 2, article e0341722, 2023.

[39] L. M. Wright, E. M. Carpinone, T. L. Bennett, M. K. Hondalus, and V. J. Starai, "VapA of *Rhodococcus equi* binds phosphatidic acid," *Molecular Microbiology*, vol. 107, no. 3, pp. 428–444, 2018.

[40] A. P. Rofe and P. R. Pryor, "Purification of lysosomes using supraparamagnetic iron oxide nanoparticles (SPIONs)," *Cold Spring Harbor Protocols*, vol. 4, 2016.

[41] J. Canton and S. Grinstein, "Measuring lysosomal pH by fluorescence microscopy," *Methods in Cell Biology*, vol. 126, pp. 85–99, 2015.

[42] A. A. Miranda-CasoLuengo, R. Miranda-CasoLuengo, N. T. Lieggi, H. Luo, J. C. Simpson, and W. G. Meijer, "A real-time impedance based method to assess *Rhodococcus equi* virulence," *PLoS One*, vol. 8, no. 3, article e60612, 2013.

[43] D. E. Johnson, P. Ostrowski, V. Jaumouillé, and S. Grinstein, "The position of lysosomes within the cell determines their luminal pH," *The Journal of Cell Biology*, vol. 212, no. 6, pp. 677–692, 2016.

[44] N. A. Bright, L. J. Davis, and J. P. Luzio, "Endolysosomes are the principal intracellular sites of acid hydrolase activity," *Current Biology*, vol. 26, no. 17, pp. 2233–2245, 2016.

[45] S. Guha, E. E. Coffey, W. Lu et al., "Approaches for detecting lysosomal alkalinization and impaired degradation in fresh and cultured RPE cells: evidence for a role in retinal degenerations," *Experimental Eye Research*, vol. 126, pp. 68–76, 2014.

[46] M. J. Mahon, "pHluorin2: an enhanced, ratiometric, pH-sensitive green florescent protein," *Advances in Bioscience and Biotechnology*, vol. 2, no. 3, pp. 132–137, 2011.

[47] K. Kim, H. Yoon, M. Diez-Silva, M. Dao, R. R. Dasari, and Y. Park, "High-resolution three-dimensional imaging of red blood cells parasitized by plasmodium falciparum and in situ hemozoin crystals using optical diffraction tomography," *Journal of Biomedical Optics*, vol. 19, no. 1, article 011005, 2014.

[48] T. Haubenthal, P. Hansen, I. Krämer et al., "Specific preadaptations of *Rhodococcus equi* cooperate with its virulence-associated protein a during macrophage infection," *Molecular Microbiology*, vol. 119, no. 3, pp. 285–301, 2023.

[49] J. A. Mindell, "Lysosomal acidification mechanisms," *Annual Review of Physiology*, vol. 74, no. 1, pp. 69–86, 2012.

[50] V. Riazanski, G. Mauleon, A. M. Zimnicka, S. Chen, and D. J. Nelson, "Phagosomal chloride dynamics in the alveolar macrophage," *iScience*, vol. 25, no. 1, article 103636, 2022.

[51] A. Di, M. E. Brown, L. V. Deriy et al., "CFTR regulates phagosome acidification in macrophages and alters bactericidal activity," *Nature Cell Biology*, vol. 8, no. 9, pp. 933–944, 2006.

[52] A. R. Graves, P. K. Curran, C. L. Smith, and J. A. Mindell, "The Cl-/H+ antiporter ClC-7 is the primary chloride permeation pathway in lysosomes," *Nature*, vol. 453, no. 7196, pp. 788–792, 2008.

[53] B. E. Steinberg, K. K. Huynh, A. Brodovitch et al., "A cation counterflux supports lysosomal acidification," *The Journal of Cell Biology*, vol. 189, no. 7, pp. 1171–1186, 2010.

[54] P.-H. Lin, P. Duann, S. Komazaki et al., "Lysosomal two-pore channel subtype 2 (TPC2) regulates skeletal muscle autophagic signaling," *The Journal of Biological Chemistry*, vol. 290, no. 6, pp. 3377–3389, 2015.

[55] J. Z. Wu, M. Zeziulia, W. Kwon, T. J. Jentsch, S. Grinstein, and S. A. Freeman, "ClC-7 drives intraphagosomal chloride accumulation to support hydrolase activity and phagosome resolution," *The Journal of Cell Biology*, vol. 222, no. 6, 2023.

[56] V. Kalatzis, S. Cherqui, C. Antignac, and B. Gasnier, "Cystinosin, the protein defective in cystinosis, is a H(+)-driven lysosomal cystine transporter," *The EMBO Journal*, vol. 20, no. 21, pp. 5940–5949, 2001.

[57] C. Sagné, C. Agulhon, P. Ravassard et al., "Identification and characterization of a lysosomal transporter for small neutral amino acids," *Proceedings of the National Academy of Sciences of the United States of America*, vol. 98, no. 13, pp. 7206–7211, 2001.

[58] M. Hu, J. Chen, S. Liu, and H. Xu, "The acid gate in the lysosome," *Autophagy*, vol. 19, no. 4, pp. 1368–1370, 2023.

[59] W. Zheng, C. Shen, L. Wang et al., "pH regulates potassium conductance and drives a constitutive proton current in human TMEM175," *Science Advances*, vol. 8, no. 12, article eabm1568, 2022.